

## Oscillatory forcing of flow through porous media. Part 2. Unsteady flow

By D. R. GRAHAM AND J. J. L. HIGDON

Department of Chemical Engineering, University of Illinois, Urbana, IL 61801, USA

(Received 5 November 1998 and in revised form 27 December 2001)

Numerical computations are employed to study the phenomenon of oscillatory forcing of flow through porous media. The Galerkin finite element method is used to solve the time-dependent Navier–Stokes equations to determine the unsteady velocity field and the mean flow rate subject to the combined action of a mean pressure gradient and an oscillatory body force. With strong forcing in the form of sinusoidal oscillations, the mean flow rate may be reduced to 40% of its unforced steady-state value. The effectiveness of the oscillatory forcing is a strong function of the dimensionless forcing level, which is inversely proportional to the square of the fluid viscosity. For a porous medium occupied by two fluids with disparate viscosities, oscillatory forcing may be used to reduce the flow rate of the less viscous fluid, with negligible effect on the more viscous fluid. The temporal waveform of the oscillatory forcing function has a significant impact on the effectiveness of this technique. A spike/plateau waveform is found to be much more efficient than a simple sinusoidal profile. With strong forcing, the spike waveform can induce a mean axial flow in the absence of a mean pressure gradient. In the presence of a mean pressure gradient, the spike waveform may be employed to reverse the direction of flow and drive a fluid against the direction of the mean pressure gradient. Owing to the viscosity dependence of the dimensionless forcing level, this mechanism may be employed as an *oscillatory filter* to separate two fluids of different viscosities, driving them in opposite directions in the porous medium. Possible applications of these mechanisms in enhanced oil recovery processes are discussed.

---

### 1. Introduction

In Part 1 (Graham & Higdon 2002), we discussed the concept of oscillatory forcing for enhanced transport of single-phase fluids flowing through porous media. We studied the steady flow behaviour as a function of Reynolds number for two simple geometrical models consisting of constricted channels and periodic arrays of circular cylinders. For steady flows, we showed that inertial forces play a critical role in determining the flow resistance and introduce a nonlinear dependence between the flow rate and applied forcing level.

Here, in Part 2, our goal is to conduct a detailed study of the unsteady flows associated with oscillatory forcing of porous media. In Part 1, we briefly discussed methods by which the oscillatory forcing might be introduced into the porous medium. In a manufacturing setting these methods might include mechanical oscillation of the entire medium or oscillatory motion associated with a travelling wave induced by mechanically driven oscillators or ultrasonic transducers. When the porous medium

is of large extent, such as in a petroleum reservoir, the oscillatory forcing must be introduced by wave propagation through the medium.

The propagation of acoustic waves in fluid-saturated porous media has been the subject of much study in the literature dating from the early work of Biot (1956*a, b*). Chapman & Higdon (1992, 1994) present a review of recent work covering the theory for the dynamics of both the fluid and solid phases. We assume that the porous medium is a porous elastic solid in which a travelling acoustic wave is introduced by external stimulus. For acoustic wavelengths which are large compared to the characteristic pore size, the coupling of the fluid dynamics and the solid mechanics is significantly simplified. The long-distance wave propagation occurs primarily through the elastic deformation in the solid phase, while the fluid motion acts as a relatively short-range damping force. The acoustic wave induces a large-scale motion of the solid phase which provides an accelerating reference frame for the microscopic fluid motion. On the microscopic scale, asymptotic analysis shows that fluid-phase compressibility effects are negligible, and the flow is incompressible (Burrige & Keller 1981). For the fluid motion on this scale, the governing equations reduce to those for an incompressible fluid flowing through a rigid porous medium with an oscillatory body force accounting for the action of the accelerating reference frame. With this background, we infer that the effects of acoustic stimulation on porous media may be studied by considering pore-scale fluid flows subject to the simultaneous action of a mean pressure gradient and an oscillatory body force. The mean pressure gradient arises from the pumping action or constant pressure head in the system, while the oscillatory body force arises from the acoustic stimulation.

In our study, we adopt simple geometric models for the porous microstructure; in particular, we consider the two-dimensional constricted channels and cylinder arrays introduced in Part 1. A number of prior studies have been devoted to oscillatory flow in constricted channels with geometry similar to the models employed here. Sobey and coworkers (Sobey 1980; Stephanoff, Sobey & Bellhouse 1980) conducted a computational and experimental study of oscillatory flow in two-dimensional channels to investigate the high rates of convective mass transfer arising in such flows. They showed that large vortices develop in the expanded part of the channel and provide the strong transverse mixing required for efficient mass transfer. Ralph (1986) studied oscillatory flow in axisymmetric constricted tubes and found a number of flow patterns similar to those shown by Sobey. In addition, Ralph studied a previously neglected range of Strouhal numbers and discovered a new class of asynchronous flows which did not match the time periodicity of the oscillatory driving force. In a similar study, Roberts & Mackley (1996) considered flow through baffled channels and showed that initially symmetric time-periodic solutions become asymmetric time-aperiodic and eventually chaotic as the oscillatory Reynolds number increases. Nishimura (1995) performed calculations on asymmetric channels and showed vortex formation and mass transfer enhancement similar to that found in symmetric channels.

While the researchers above have focused on the flow morphology in oscillatory flow, there has been relatively little study of the relationship between the flow rate and the magnitude of the oscillatory driving force. In the absence of nonlinear inertial effects, the flow is governed by the unsteady Stokes equations, and there is a linear relationship between the flow rate and pressure gradient. The complex-valued coefficient of proportionality is a frequency-dependent quantity known as the dynamic permeability. Chapman & Higdon (1992) give an extensive review of the literature on dynamic permeability and present detailed computational results for

three-dimensional models of porous media. Owing to the linearity of the unsteady Stokes regime, however, the fluid velocity is strictly oscillatory, and the oscillatory pressure gradient has no effect on the mean flow.

On reviewing the extensive research on flow in porous media, we find no work which directly examines the effect of oscillatory forcing on the mean flow rate. Previous efforts have been limited to unsteady Stokes flow or to studies of the flow patterns in oscillatory motion. In the present paper, we examine the flow fields arising in response to the simultaneous action of a mean pressure gradient and an oscillatory driving force. Our goal is to investigate the physical mechanisms responsible for enhanced transport in oscillatory forcing of flow in porous media. In pursuit of this goal, we present an extensive series of results based on unsteady solutions of the time-dependent Navier–Stokes equations. We show that the introduction of an oscillatory pressure force may act either to enhance or to retard the mean flow rate. We conduct a parametric study on the influence of the oscillatory pressure forces and determine the effects of the amplitude, frequency and temporal waveform of the oscillatory driving force.

## 2. Problem description and numerical methods

The two geometric models considered in this paper include sinusoidal constricted channels and periodic lattices of circular cylinders. The geometry and parameters for these models are defined in Part 1 and illustrated in figures 1 and 2 therein. The constricted channels are parameterized by the wall slope  $ak$  and the dimensionless gap size  $h/a$ . The cylinder arrays are parameterized by the ratio  $h/r$  where  $r$  is the cylinder radius.

The governing equations for the fluid flow are the two-dimensional incompressible Navier–Stokes equations together with the continuity equation:

$$\rho \left( \frac{\partial \mathbf{u}}{\partial t} + \mathbf{u} \cdot \nabla \mathbf{u} \right) = -\nabla P + \mu \nabla^2 \mathbf{u} + \mathbf{b}, \quad (2.1)$$

$$\nabla \cdot \mathbf{u} = 0. \quad (2.2)$$

The boundary conditions are no slip on the boundary walls and periodicity at the inlet and outlet, identical to those imposed in Part 1.

The body force in the Navier–Stokes equations is the sum of a mean component  $\mathbf{G}_o$  and an oscillatory component  $\mathbf{G}_\omega$ :

$$\mathbf{b} = \mathbf{G}_o + \mathbf{G}_\omega(t). \quad (2.3)$$

The mean component represents the imposed mean pressure gradient (see Part 1), and the oscillatory component represents either an oscillatory pressure gradient or the action of an accelerating reference frame (e.g. acoustic stimulation). As in Part 1, we non-dimensionalize all quantities with respect to the parameters  $h$ ,  $\rho$  and  $\nu$ , where  $h$  is the gap size of the constriction,  $\rho$  is the fluid density and  $\nu$  is the kinematic viscosity. The dimensionless body forces are designated as  $\mathbf{F}_o$  and  $\mathbf{F}_\omega$  where

$$\mathbf{F}_o = \mathbf{G}_o h^3 / \rho \nu^2, \quad \mathbf{F}_\omega = \mathbf{G}_\omega h^3 / \rho \nu^2. \quad (2.4)$$

As in the steady case, we break  $\mathbf{F}_o$  and  $\mathbf{F}_\omega$  into  $x$ - and  $y$ -components designated  $F_{x_o}$ ,  $F_{y_o}$  and  $F_{x_\omega}$ ,  $F_{y_\omega}$  respectively. The frequency  $f$  of the forcing is non-dimensionalized

with respect to viscosity and gap size yielding the dimensionless frequency

$$\Omega = fh^2/\nu. \quad (2.5)$$

The fluid flow rate or spatial average fluid velocity is defined as

$$U(t) = \frac{1}{2h} \int_{-h}^h \mathbf{u}(t) \cdot \mathbf{n} \, dS \quad (2.6)$$

and its long-term time average is defined by

$$\bar{U} = \lim_{t_2 \rightarrow \infty} \frac{1}{t_2 - t_1} \int_{t_1}^{t_2} U(t) \, dt. \quad (2.7)$$

The dimensionless mean flow rate takes the form of a Reynolds number given by

$$\bar{Re} = \frac{\bar{U}h}{\nu}. \quad (2.8)$$

In assessing the effects of oscillatory forcing on the average flow rate, we are most interested in the dependence of  $\bar{Re}$  on the parameters  $F_o$ ,  $F_\omega$ ,  $\Omega$ ,  $ak$  and  $h/a$ .

The unsteady partial differential equations (2.1) and (2.2) are solved by using the Galerkin finite element method. All details with respect to the implementation and discretization are as described in Part 1. For unsteady-state problems, the introduction of the finite-element approximations for velocity and pressure leads to a system of nonlinear differential algebraic equations. These equations are integrated in time to obtain the velocity field at successive time steps. The integration is performed with an explicit Adams–Bashforth prediction, followed by an implicit trapezoidal rule correction, as described by Gresho, Lee & Sani (1980). We employ the adaptive time step algorithm described by Gresho *et al.* with a relative error tolerance of  $10^{-3}$ . For flows with rapid flow changes, additional computations were performed to confirm that the dynamics were adequately resolved. In all cases, the smaller time step results were indistinguishable from those achieved with the base adaptive time step algorithm. The velocity fields for the initial time steps were obtained from steady-state calculations at  $F_{x0}$ .

### 3. Results

In Part 1, we characterized the flow patterns arising in steady flow, and determined the mean flow rate as a function of the forcing level  $F_o$ . In that paper, we identified three mechanisms by which oscillatory forcing might exploit the nonlinearity associated with inertial forces and achieve a net change in the mean flow rate. In this paper, we present detailed results illustrating these mechanisms, and we investigate the changes in the fluid flow resulting from the unsteady inertial forces.

We begin by considering flow in constricted channels for which the effective body force has a single component  $b_x(t)$  along the axis of the channel. For constant density fluids, oscillations perpendicular to this axis induce linear hydrostatic pressure fields with no effect on the fluid motion. For channels of fixed geometry, the three parameters which affect the flow field are the magnitudes of the mean force and oscillatory driving force and the dimensionless frequency  $\Omega = fh^2/\nu$ . The frequency  $\Omega$  represents the ratio of the viscous time scale  $h^2/\nu$  to the time scale of the oscillation  $1/f$ . When  $\Omega \ll 1$ , the driving force changes very slowly with time, and the instantaneous flow field is exactly that predicted by steady-state calculations at the same level of forcing.

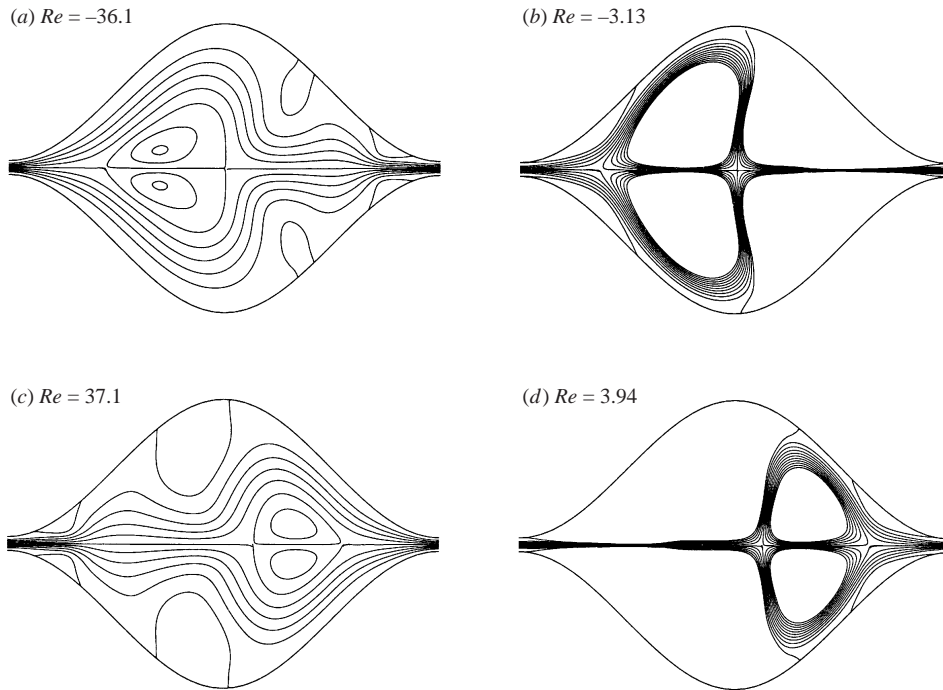


FIGURE 1. Instantaneous streamline patterns for strong oscillatory forcing  $F_{xo} = 20$  in the presence of a small mean pressure gradient  $F_{xo} = 0.25$  at frequency  $\Omega = 0.25$ . Images show flow at successive instants in time during a cycle. The direction of the flow is indicated by the sign of the Reynolds number; negative indicating right to left and positive indicating left to right.

For oscillatory flows in this *quasi-steady* regime, the mean flow rate may be calculated directly from the steady state results of Part 1.† A major goal of the current effort will be to compare the predictions of quasi-steady theory with the computed results for unsteady flows and thereby to characterize the influence of the dimensionless frequency  $\Omega$ .

### 3.1. Sinusoidal forcing

For our first series of unsteady computations, we consider a simple sinusoidal time dependence represented by a single Fourier mode with

$$b_x(t) = F_{xo} + F_{xo} \sin(2\pi ft). \quad (3.1)$$

For low forcing frequencies, the flow field is consistent with that predicted by the steady-state results in Part 1. To illustrate the changes occurring at higher frequencies, we choose  $\Omega = 0.25$  and present the flow patterns for several different forcing levels. We consider a constricted channel with  $ak = 1$  and  $h/a = 0.1$  subject to a low level of mean forcing  $F_{xo} = 0.25$ . Instantaneous streamline patterns at several points during one cycle of forcing are shown in figure 1, for conditions where the oscillatory forcing  $F_{xo} = 20$  is much stronger than the mean forcing. For these conditions, the oscillatory component of the forcing is strong enough to reverse the flow direction for part of

† For flows with bifurcations to multiple stable steady solutions, the quasi-steady analysis cannot discern which branch the unsteady flow would select. In the present circumstances, all flows with multiple stable solutions involve mirror image solutions and the flow rates are identical independent of the branch selected. In more general geometries, this will not always be the case.

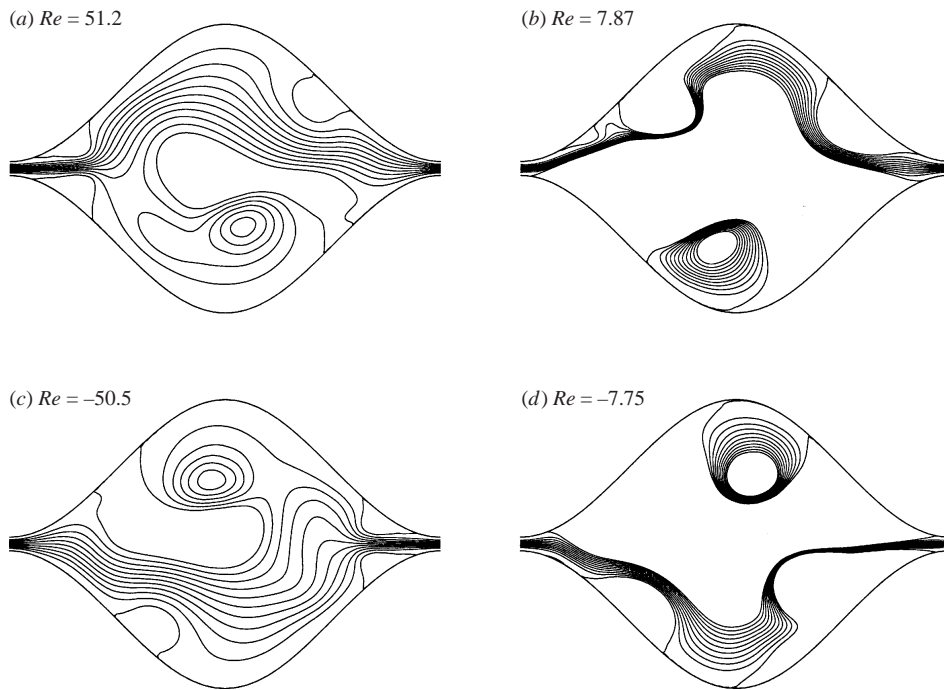


FIGURE 2. Instantaneous streamline patterns for  $F_{x\omega} = 30$ ,  $F_{x\sigma} = 0.25$ , and  $\Omega = 0.25$  at successive instants in time during a cycle. The direction of the flow is indicated by the sign of the Reynolds number; negative indicating right to left and positive indicating left to right.

the cycle. Throughout the forcing cycle, flow patterns maintain symmetry and are characterized by the presence of a vortex pair in the expanded part of the channel. As the magnitude of the oscillatory forcing is increased to  $F_{x\omega} = 30$ , the flow structure changes dramatically, as illustrated in figure 2. At this forcing level, the flow is no longer symmetric, and the streamline patterns show significant variation from one cycle to the next. The flow behaviour for  $F_{x\omega} = 30$  is aperiodic and chaotic, consistent with previous studies showing aperiodic motion at higher flow rates. Note that the instantaneous streamline patterns for a single cycle (figure 2) are insufficient to confirm the aperiodic nature of this flow. This conclusion is based on streamline patterns taken over many cycles and is confirmed by the data for the average flow rate discussed below. A further increase in the magnitude of the oscillatory forcing to  $F_{x\omega} = 40$  results in the flow patterns shown in figure 3. In this case, the flow is asymmetric, and the streamline patterns from successive cycles are similar. The variations in the velocity field are synchronized with the cycle of the oscillatory driving force. Each of the streamline patterns in figure 3 bears a strong resemblance to the stable asymmetric steady flows seen in Part 1. In each of these flows, a large eddy occupies the centre of the channel, while a concentrated jet of fluid flows along one of the channel walls. When the flow changes direction, the jet on one wall decays, and a jet moving in the opposite direction forms on the opposing wall. With the alternating jet positions, the large centre eddy maintains the same sense of rotation throughout the entire cycle. It is this large mass of rotating fluid which imposes order on the unsteady motion and ensures a consistent repetition of the flow pattern from one cycle to the next.

In summary, we have seen two distinct temporally periodic flow patterns develop in

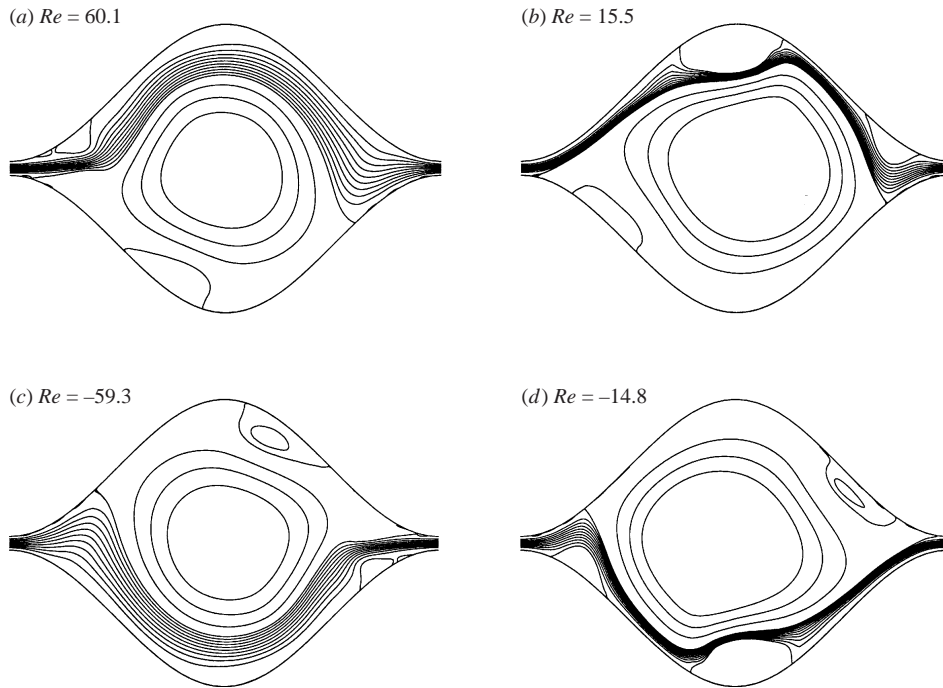


FIGURE 3. Instantaneous streamline patterns for  $F_{x\omega} = 40$ ,  $F_{x_0} = 0.25$ , and  $\Omega = 0.25$  at successive instants in time during a cycle. The direction of the flow is indicated by the sign of the Reynolds number; negative indicating right to left and positive indicating left to right.

the constricted channel. For forcing levels up to  $F_{x\omega} = 20$ , a symmetric flow develops with vortex pairs propagating along the channel in opposite directions during different parts of the cycle. For forcing levels of  $F_{x\omega} = 40$  and larger, an asymmetric flow develops with concentrated jets along the walls and a single large eddy in the centre of the channel. At intermediate forcing levels such as  $F_{x\omega} = 30$ , the flow is unable to sustain a consistent oscillation in either mode and a chaotic temporally aperiodic motion ensues. In presenting these results, we note that the streamline patterns at the forcing levels shown here are representative of the types of flow structure which may develop. The transitions from one flow pattern to the next are governed by both the forcing level and the frequency of the stimulation. We shall return to this issue in the discussion of the frequency dependence later in this section.

Having illustrated the flow patterns observed for oscillatory flow, we now consider the effect of the oscillatory component of forcing on the mean flow rate. One useful measure of the average flow rate is the one-cycle average,

$$\overline{Re} = \frac{1}{T} \int_{t_1}^{t_1+T} Re(t) dt, \quad (3.2)$$

where  $T$  is the period of the oscillatory forcing. This quantity has been calculated for each cycle of the unsteady simulations, and results for several forcing levels are shown in figure 4. For forcing levels of  $F_{x_0} = 20$  and  $F_{x_0} = 40$ , the one-cycle average  $\overline{Re}$  experiences at most a brief initial fluctuation and rapidly settles down to a constant value which is maintained for an indefinite period. These results are consistent with the periodic time behaviour observed in the streamline plots for these forcing levels. By contrast, the one-cycle averages for  $F_{x\omega} = 30$  show large random fluctuations over

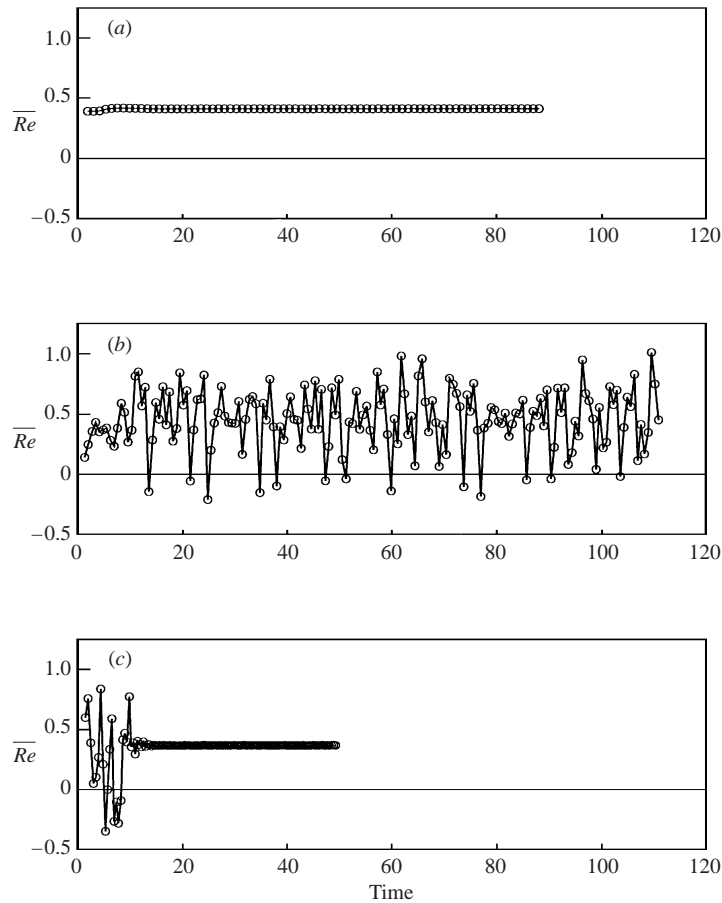


FIGURE 4. Average Reynolds number computed over one cycle vs. time. Time is non-dimensionalized with the period of the forcing. The conditions are  $F_{x0} = 0.25$ ,  $\Omega = 0.25$ , and (a)  $F_{x\omega} = 20$ , (b)  $F_{x\omega} = 30$ , (c)  $F_{x\omega} = 40$ .

more than 100 cycles of oscillation with no sign of convergence to a constant value. This type of time-aperiodic flow is similar to that observed by Roberts & Mackley (1996) for flow through a baffled channel. The one-cycle averages in figure 4 show no obvious sign of subharmonic periodicity; this fact can be confirmed by evaluating the Fourier coefficients for the entire 100-period data set for  $Re(t)$ . Figures 5(a) and 5(b) show the magnitude of the Fourier coefficients as a function of frequency. Figure 5(a) shows that the coefficient associated with the forcing frequency is much larger than the other coefficients, which lie nearly on the horizontal axis in this figure. The Fourier coefficients for the subharmonic frequencies are shown on an expanded scale in figure 5(b). The subharmonic coefficients are much smaller in magnitude than the coefficient associated with the forcing frequency, and they show broad coverage over all frequencies with no evidence of a dominant oscillation mode at any distinct subharmonic frequency. This conclusion is consistent with our earlier observations of the streamline patterns, confirming the chaotic nature of the flow at intermediate forcing levels.

When the  $\overline{Re}$  based on one-cycle averages changes significantly over successive

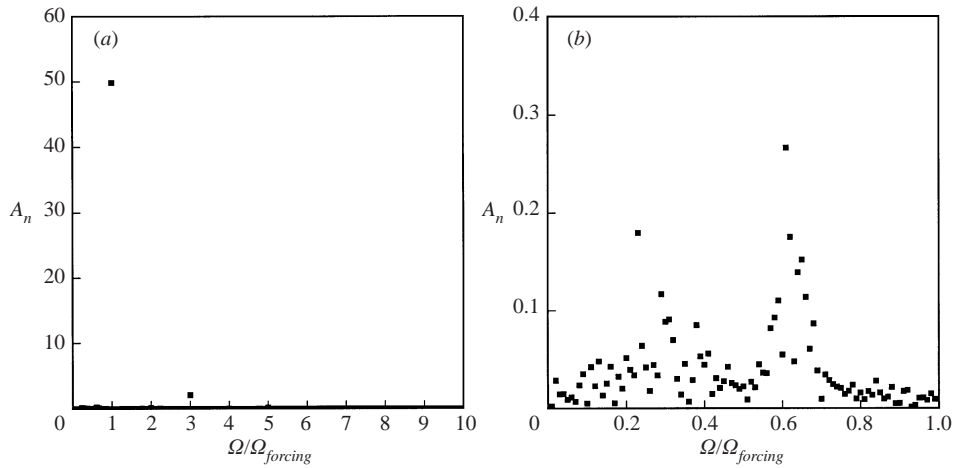


FIGURE 5. Magnitude of Fourier coefficients as a function of frequency for  $F_{x\omega} = 30$ ,  $F_{x0} = 0.25$  and  $\Omega = 0.25$ .  $A_n = \sqrt{a_n^2 + b_n^2}$  where  $a_n$  and  $b_n$  are defined such that  $Re(t) - \overline{Re} = \sum_{n=1}^{\infty} [a_n \cos(2\pi f t) + b_n \sin(2\pi f t)]$ .

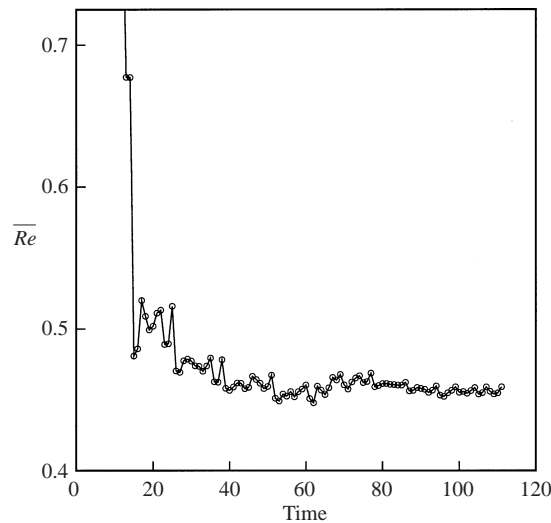


FIGURE 6. Long-time average flow rate as defined in equation (3.3) with  $t_1 = 10$  periods for  $F_{x0} = 0.25$ ,  $\Omega = 0.25$  and  $F_{x\omega} = 30$ .

cycles, a more meaningful flow measure is the long-term average defined by

$$\overline{Re} = \lim_{t \rightarrow \infty} \frac{1}{t - t_1} \int_{t_1}^t Re(t) dt, \tag{3.3}$$

where the integration begins at some finite value  $t_1$  to exclude the effects of initial transients. Figure 6 shows the behaviour of the long-term average for the chaotic flow at forcing level  $F_{x\omega} = 30$ . The fluctuations for this average are significantly smaller than the variations in the one-cycle averages and converge to a steady mean. On a computational note, we observe that the accurate calculation of the long-term average for chaotic flows such as that shown in figure 6 require significantly longer simulations than for the well-behaved periodic flows.

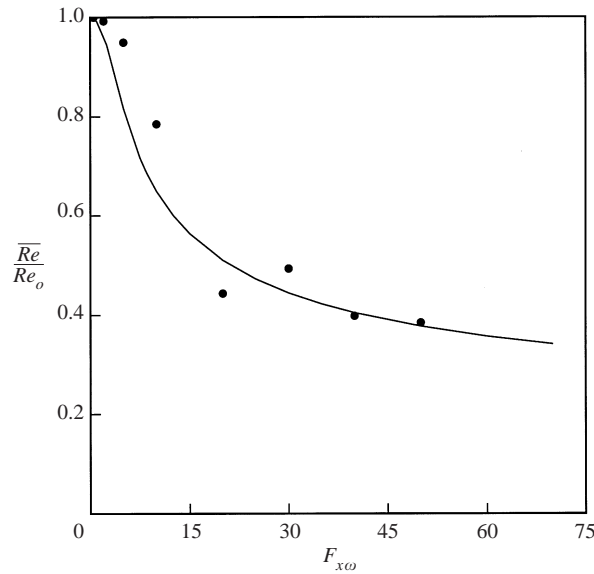


FIGURE 7. Mean flow rate as a function of oscillatory forcing for  $F_{x0} = 0.25$ . The solid line indicates quasi-steady analysis and the symbols are results of unsteady simulations at  $\Omega = 0.25$ .

With a well-defined procedure for computing the average flow rate in unsteady flows, we now consider the effect of the oscillatory forcing parameters on the mean flow rate. We recall that predictions for the mean flow rate at low oscillation frequencies may be obtained from steady-state data by employing a quasi-steady model. The quasi-steady prediction is given by

$$\overline{Re} = \frac{1}{T} \int_{t_1}^{t_1+T} Re_o(F) dt, \quad (3.4)$$

where  $Re_o(F)$  is the steady-state flow rate at the instantaneous forcing level  $F$ , and  $F(t)$  is a prescribed function of time.

The mean flow rate subject to the action of a mean pressure gradient and an oscillatory driving force is shown in figure 7. The flow rate is plotted as a function of oscillatory forcing level with the circles showing results from unsteady simulations and the solid line showing a quasi-steady prediction. The mean pressure gradient  $F_{x0} = 0.25$  and the frequency  $\Omega = 0.25$  are the same as for the streamline patterns illustrated in figures 1–3. Both the unsteady calculations and the quasi-steady analysis show that the average flow rate decreases as the oscillatory forcing level is increased, with a substantial reduction when the oscillatory forcing  $F_{x\omega}$  is much stronger than  $F_{x0}$ .

The explanation for this phenomenon is revealed by considering the nonlinear effects of inertial forces as seen in the steady-state calculations. Figure 8 shows the steady flow rate as a function of driving force for the stable solution branch of the steady bifurcation diagram for this channel geometry. The dashed line shows the extrapolated result from the low Reynolds number or Darcy flow regime. With an oscillatory driving force in the quasi-steady limit, the flow will sample a range of instantaneous forces as shown by the inset in the figure. For the Darcy flow line, the velocity is related to the force by a constant coefficient  $C$ ,

$$U(t) = C[F_{x0} + F_{x\omega} \sin(2\pi ft)], \quad (3.5)$$

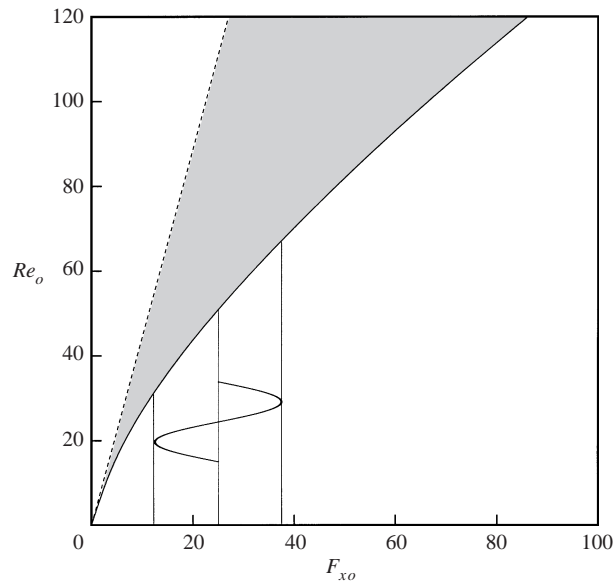


FIGURE 8. Illustration of quasi-steady analysis. The dotted line is the Stokes flow or Darcy's law prediction and the solid line is the computed steady flow result. The inset shows an example of an unsteady forcing function.

and the average flow reduces to the steady value with no effect of the oscillatory forcing. Owing to the inertial effects however, the actual flow rate falls below the Darcy prediction, and the large forcing levels produce significantly less flow than a linear extrapolation predicts. The flow deficit at large forcing is shown by the shaded region between the two curves. When averaged over one cycle, the negative part of the oscillatory cycle yields smaller driving forces and less inertial drag than the positive part of the cycle. With a greater flow penalty in the positive part of the cycle, the net effect is to reduce the mean flow rate below that achieved with a steady mean forcing.

Further examination of the unsteady results in figure 7 shows the effect of the transition from symmetric flows to asymmetric flows. For  $F_{x\omega}$  between 5 and 20, the velocity field is symmetric, and the flow rate decreases sharply owing to the inertial losses induced by the vortex pairs in the centre of the channel. This sharp decrease ceases suddenly at  $F_{x\omega} = 30$ , corresponding to the transition between the symmetric and asymmetric flow. For higher  $F_{x\omega}$ , the flow is asymmetric and  $\overline{Re}$  decreases less rapidly with increasing forcing level. In this regime, the flow patterns closely match their steady-state counterparts, and the quasi-steady predictions show excellent agreement with the unsteady simulations.

Given the dramatic reduction in mean flow rate produced by strong oscillatory forcing, we see that oscillatory forcing may have a significant effect on transport in fluid-saturated porous media. As one example, we examine the case of acoustic stimulation for improving the efficiency of secondary oil recovery. Consider a reservoir where extended patches are occupied by a single-phase fluid with separate regions for the water phase and for the oil phase. In these regions, each phase is subject to an oscillatory body force  $b_{x\omega}$  which is proportional to the density of the fluid and the acceleration of the solid matrix. While each phase experiences nearly the same dimensional forcing level  $b_{x\omega}$ , the dimensionless forcing level  $F_{x\omega} = b_{x\omega}h^3/\rho v^2$  is much

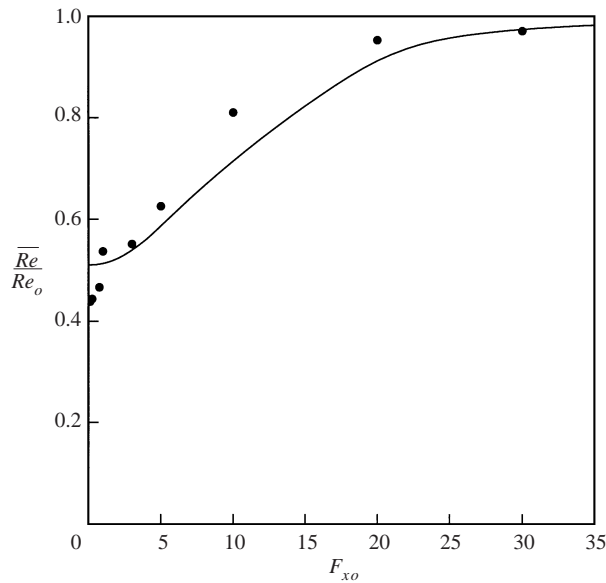


FIGURE 9. Mean flow rate  $\overline{Re}/Re_o$  as a function of steady forcing level  $F_{x_o}$  for a fixed level of oscillatory forcing. The circles represent unsteady calculations for  $F_{x_{\omega}} = 20$  and  $\Omega = 0.25$  and solid line represents quasi-steady analysis.

higher for the water phase owing to its smaller viscosity. One may choose a forcing level  $b_{x_{\omega}}$  such that there is a significant reduction in  $\overline{Re}/Re_o$  for the water, while the flow rate of the oil is essentially unchanged. In simple physical terms, the inertial forces would play a significant role in the water phase while having negligible effect in the more viscous oil phase. The net result of the process is to increase the speed of the oil relative to the water, leading to a higher concentration of oil in the product stream.

We have seen the effect of varying the level of oscillatory forcing while holding the mean pressure gradient constant. To further characterize the effect of flow parameters on the average flow rate, figure 9 shows the results of setting a fixed level of oscillatory forcing and varying the strength of the steady forcing  $F_{x_o}$ . In this figure, we observe that a significant reduction in flow rate is achieved for arbitrarily small steady forcing levels. As the level of steady forcing increases however, the effect of the oscillatory forcing diminishes, and the mean flow rate approaches the steady-state value. At equal levels of mean and oscillatory forcing, the mean flow rate is approximately 95% of its steady-state value. Thus we find that the level of oscillatory forcing must be significantly greater than the steady forcing level to have a meaningful effect. As with our earlier results, we note that the quasi-steady analysis predicts the correct trends for the unsteady calculations.

The final parameter to be considered in this section is the frequency of oscillation,  $\Omega$ . This parameter is significant, because the strength of the oscillatory driving force  $b_{x_{\omega}}$  is proportional to the amplitude of the displacement wave and the square of its frequency. The delivery of strong oscillatory forcing to porous media is facilitated if high frequencies can be employed and proportionately smaller amplitudes may be utilized. Figure 10 shows the flow rate as a function of the dimensionless frequency for a system with strong oscillatory forcing. In this figure, we observe that the oscillatory forcing produces a significant effect on the mean flow rate for frequencies in the range

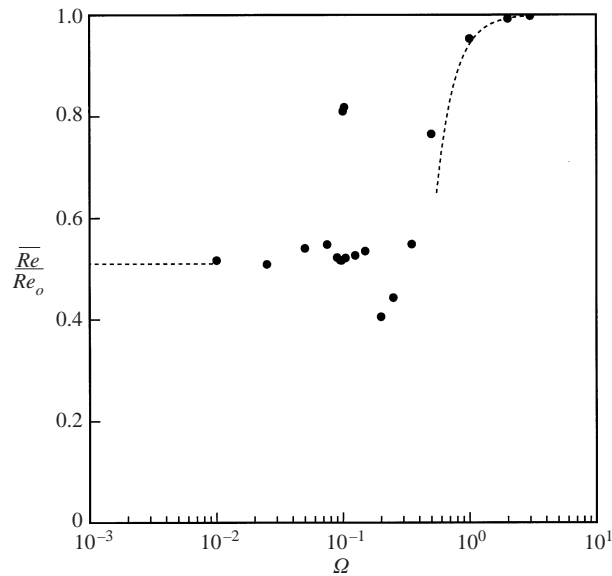


FIGURE 10. Mean flow rate  $\bar{Re}/Re_o$  as a function of frequency  $\Omega$  for  $F_{xo} = 0.25$  and  $F_{xo} = 20$ . The dashed lines are described in the text.

$0 \leq \Omega \leq 0.50$ . Above this frequency range, the effect of the oscillatory forcing rapidly diminishes, because the fluid velocity has insufficient time to respond to the imposed oscillation. Further examination of figure 10 reveals a number of dramatic changes in the flow rate over narrow frequency bands in the range  $\Omega \approx 0.1$  and  $\Omega \approx 0.2$ . The sudden change over a narrow frequency range is an interesting phenomenon, but it has little consequence for real porous media. The frequency  $\Omega$  is non-dimensionalized with gap size  $h$ , and the phenomenon would thus occur only for gap sizes in a narrow range. Real media have a wide distribution of pore and constriction sizes which would minimize the appearance of these effects.

The overall frequency behaviour seen in figure 10 may be explained by considering the relevant time scales in this problem. There are three characteristic time scales associated with the unsteady flows driven by oscillatory forcing. The first is given by the period of the oscillatory forcing  $1/f$ . The second is the viscous diffusion time scale  $h^2/\nu$ . The ratio of these scales gives our dimensionless frequency  $\Omega$ . The third time scale is the transient scale measuring the time required for a flow starting from one forcing level (or rest) to reach a steady flow condition. During this transient, the flow shows unsteady flow characteristics including vortex pair formation and propagation similar to the streamlines shown in figure 1. This third scale is equal to the viscous diffusion time scale in parallel flows, but is more complicated in the present geometry owing to the vortex dynamics.

At very low forcing frequencies, the oscillatory time scale is much larger than both the transient and viscous time scales, and the flow pattern develops in the form of the steady-state solutions. The flow rate is as predicted by quasi-steady analysis and is shown as the horizontal dashed line on figure 10. For very high frequencies when the oscillatory time scale is much smaller than both the transient and viscous time scales, the unsteady terms in the Navier–Stokes equations dominate, and the flow character is governed by the linear unsteady Stokes equations. In this regime, the oscillatory motion and the mean flow are decoupled owing to the linearity, and the

modification of the mean flow goes to zero. The flow in the centre of the channel is irrotational, while viscous effects and vorticity are confined to oscillatory boundary layers on the channel walls. Chapman & Higdon (1992) discuss the relevant literature on this regime.

The first modification of the flow owing to nonlinear inertial effects at high frequency is the steady inertial streaming induced by Reynolds stresses. Rosenhead (1963, section VII.10) gives a review of the classic literature on this phenomenon. For geometries with fore–aft symmetry, inertial streaming induces a steady flow, but symmetry dictates that the total volume flow rate is identically zero. The first modification of the volume flow rate associated with nonlinear inertial effects enters at third order. This modification arises from the Reynolds stresses generated by the interaction of the steady inertial streaming field and the steady flow produced by the mean pressure gradient. In dimensional terms, the oscillatory velocity in the channel scales as  $u_\omega \sim G_\omega/(\rho f)$  where  $G_\omega$  is the oscillatory body force. The steady inertial streaming velocity scales as  $ku_\omega^2/f$  (Rosenhead 1963), while the steady flow associated with the mean pressure gradient  $G_o$  scales as  $G_o h^2/\mu$ . With these estimates, the Reynolds stress scales as  $kG_o G_\omega^2 h^2/(\rho f^3 \mu)$ . The Reynolds stress counters the effect of the mean pressure gradient and reduces the total flow rate. The final expression for the mean flow rate takes the form

$$\overline{Re} = Re_o \left[ 1 - O\left(\frac{khF_\omega^2}{\Omega^3}\right) \right]. \quad (3.6)$$

This expression is shown as the dashed line on figure 10 with the coefficient of the Reynolds stress chosen such that curve passes through the data point at  $\Omega = 3$  which is the highest frequency we have computed. The asymptotic theory shows that the effects of acoustic forcing fall off as  $\Omega^{-3}$  for high-frequency forcing. Numerical results for the two highest frequencies computed confirm this scaling.

For frequencies which are intermediate between the two asymptotic regimes, the transient time scale plays an important role. When the transient time scale is larger than the oscillatory time scale, the flow has insufficient time to reach the steady-state solutions. Instead, the streamlines retain their unsteady character with vortex formation and propagation as shown in figure 1. At a certain critical frequency, such as that seen in figure 10 ( $\Omega = 0.1$ ), the flow is poised at the brink of quasi-steady behaviour where the oscillatory time scale is comparable to the transient time scale. For such frequencies, the slight directional bias associated with the mean flow may alter the flow patterns such that the forward and reverse motions show different character. This phenomenon is illustrated by the streamline patterns shown in figure 11 for a frequency  $\Omega = 0.1$ . In particular, panel (e) (with positive forcing) shows the formation of a concentrated jet of fluid across the channel analogous to a steady flow solution. With negative forcing, no such jet appears, and the flow is dominated by the vortex motion. The streamlines in this figure may be contrasted with the symmetric vortex patterns shown in figure 1 for the same forcing level at a frequency  $\Omega = 0.25$ . A further confirmation of the directional asymmetry may be obtained by examining the Fourier coefficients of the flow rate  $Re(t)$ . For frequencies above the critical frequency, the first few harmonics are in phase with the fundamental, consistent with the fore–aft symmetry. For the frequencies at or very near the critical frequency, the harmonics show a distinct phase shift compared with the fundamental, yielding asymmetry in the total flow rate which is consistent with the inference drawn from the streamline patterns.

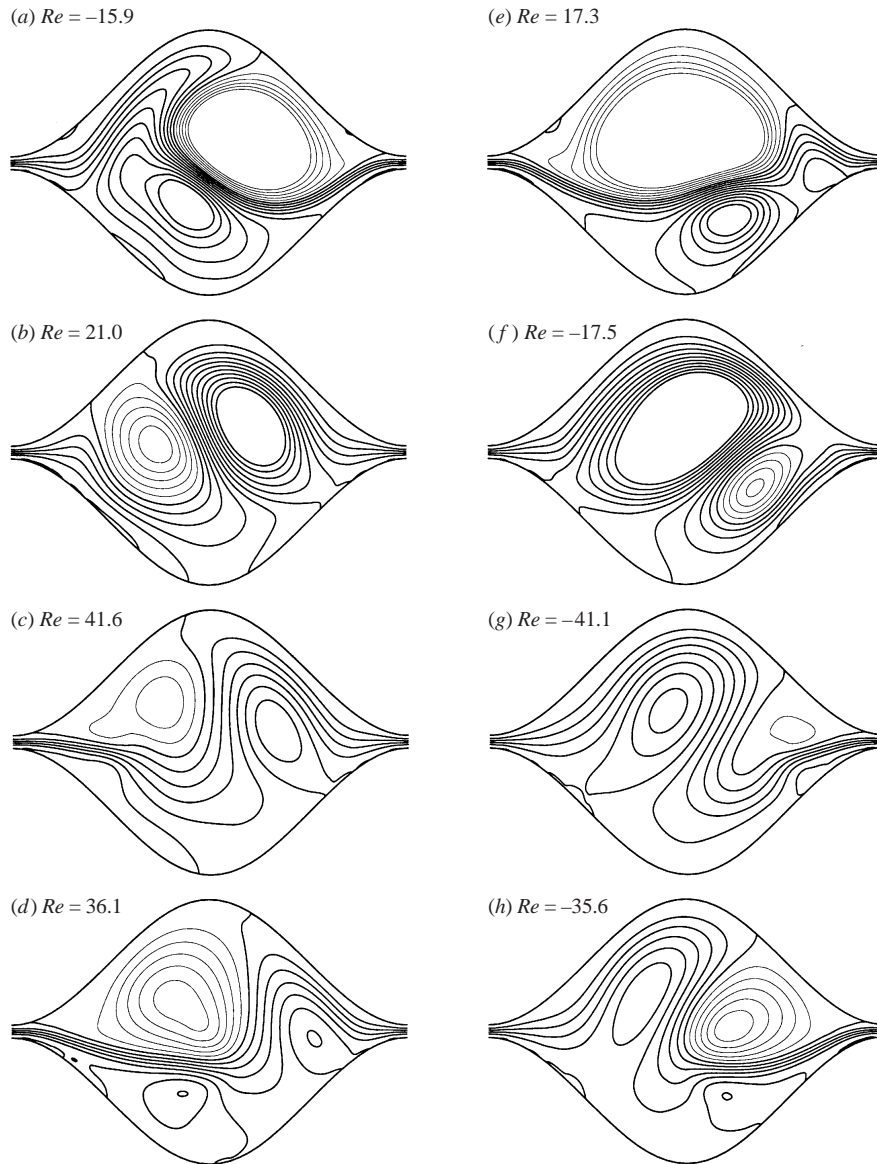


FIGURE 11. Instantaneous streamline patterns for  $F_{x0} = 20$ ,  $F_{x0} = 0.25$  and  $\Omega = 0.1$  at successive instants in time during a cycle. The direction of flow is indicated by the sign of the Reynolds number; negative indicating right to left and positive indicating left to right.

The effects of the transient time scale and the associated critical frequency may be summarized as follows. For frequencies below the critical frequency, the flow is quasi-steady with streamlines corresponding to steady-state solutions and flow rates in good agreement with the quasi-steady theory. As the forcing frequency approaches the critical frequency, there is a rapid change in flow rate as the mean flow induces a directional asymmetry in the flow patterns. It is in this frequency range that one observes the chaotic flow patterns discussed in reference to figure 4. For frequencies above the critical frequency, the flow makes a transition to periodic flow patterns characterized by vortex formation and propagation through the channel. In this range,

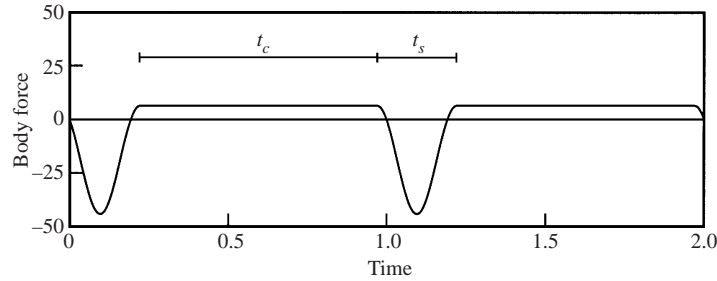


FIGURE 12. Spike waveform.

the mean flow rate reaches its minimum value owing to the inertial losses associated with the strong vortex motion. For frequencies well above the critical frequency, the flow approaches the boundary layer regime described above, the effects of the acoustic forcing fall off as  $\Omega^{-3}$ , and the mean flow rate returns to the undisturbed steady-state value.

The results presented in this section have been limited to a single channel geometry with slope  $ak = 1$  and gap size  $h/a = 0.1$ . Additional calculations have been performed for a wide range of geometric parameters as reported by Graham (1997). These calculations confirm that the changes in the mean flow rate produced by oscillatory forcing occur over a wide range of geometry, and therefore represent a promising mechanism for enhancing transport processes in porous media.

### 3.2. Non-sinusoidal forcing

The temporal waveform associated with the oscillatory forcing function has a dramatic effect on the mean flow rate through constricted channels. In previous work, we studied several different non-sinusoidal waveforms (Graham 1997) and found that the waveform with the largest impact on the mean flow rate is the spike/plateau shown in figure 12. For this waveform, the average value of the force is zero and the root-mean-square value  $F_{rms}$  provides a convenient measure of the oscillatory forcing level.

We begin our analysis by examining flows driven purely by the oscillatory spike waveform in the absence of a mean pressure gradient. Figure 13 shows the average flow rate as a function of oscillatory forcing level for both quasi-steady analysis and full unsteady simulations. In this figure, we scale the average flow rate  $\overline{Re}$  with the flow rate corresponding to steady forcing at the same r.m.s. forcing level  $F_{rms}$ . A new feature of flows driven by the spike waveform is that a mean flow is induced even when no mean forcing is imposed. The physical basis for this induced mean flow may be understood by examining the form of the forcing function. During the short spike interval  $t_s$  where the reverse forcing increases to a high level, strong inertial forces lead to a nonlinear increase in the flow resistance and a proportionally smaller increase in flow rate. For the long interval  $t_c$  with a small constant positive forcing level, the lower forcing yields less flow resistance and a proportionately higher flow rate. Averaging over one full cycle of the wave leads to a mean flow in the positive direction, even though the average forcing is equal to zero. Next, we examine the effect of the oscillation frequency  $\Omega$  on the average flow rate. Figure 14 shows that the overall frequency dependence for the spike waveform is qualitatively similar to that for the sinusoidal waves studied earlier: over a sizeable range of low frequencies,

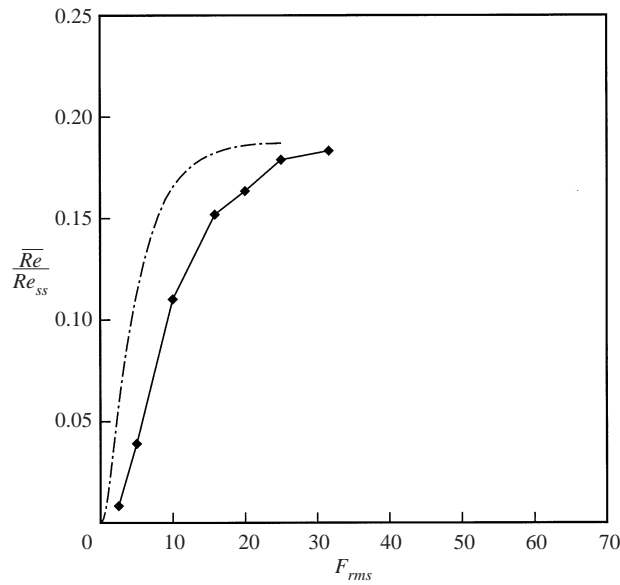


FIGURE 13. Mean flow rate as a function of oscillatory forcing level. The dashed line is the quasi-steady analysis for the spike waveform and the symbols are results from unsteady calculations at  $\Omega = 0.125$ .

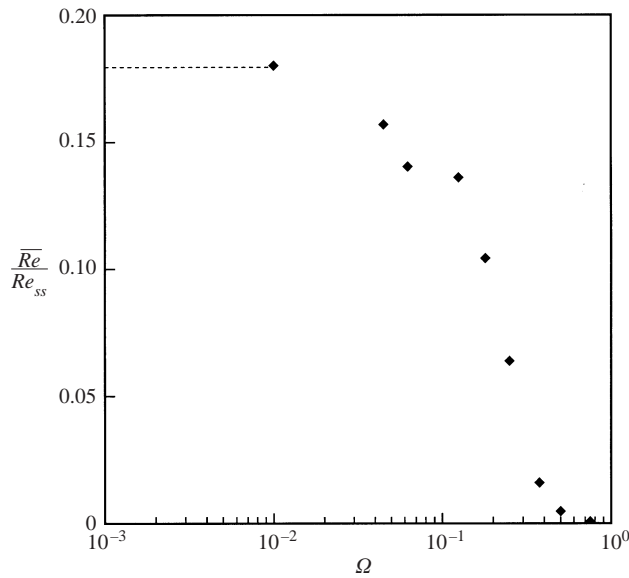


FIGURE 14. Mean flow rate as a function of frequency of oscillatory forcing for spike waveform with  $F_{x0} = 0$  and  $F_{rms} = 20/\sqrt{2}$ .

large mean flow rates are induced; however the effect decreases as the frequency is increased with negligible effects above  $\Omega = 0.50$ .

With a clear picture of the impact of spike wave forcing in the absence of a mean pressure gradient, we turn our attention to flows subject to the combined action of oscillatory and mean forcing. Given that a mean flow may be induced solely by

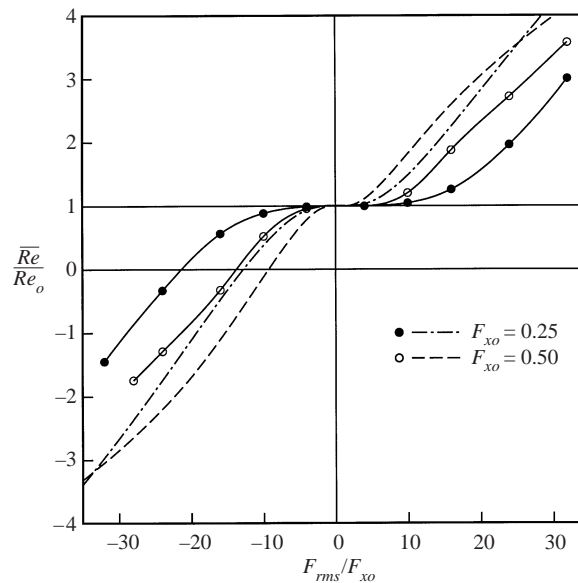


FIGURE 15. Mean flow rate as a function of the strength of the oscillatory forcing level for the spike waveform. The symbols are results from unsteady calculations at  $\Omega = 0.125$  and the dashed lines are the quasi-steady analysis. Results are presented for two levels of steady forcing  $F_{xo}$ .

oscillatory forcing, we expect a large increase in the mean flow rate when the mean and oscillatory forcing act together and a large decrease when the two are opposed. This trend is shown in figure 15, which shows results from unsteady simulations at two different levels of steady forcing. The symbols are unsteady results and the dashed lines are the quasi-steady predictions. On the right half of the figure, the steady forcing and oscillatory forcing act together, while on the left half they are in opposition. Focusing on the right-hand side, we see that the average flow rate is up to three times higher with oscillatory forcing than with steady forcing alone. Turning our attention to the left side, we see that the oscillatory forcing produces a sharp decrease in flow rate. For sufficiently high levels, the oscillatory forcing actually reverses the sense of the average flow and causes the fluid to flow against the direction of the mean pressure gradient.

In summary, we find that oscillatory forcing with spike waveforms may produce dramatic changes in the mean flow rate of fluids in porous media. As with the sinusoidal forcing discussed previously, this form of oscillatory forcing might be exploited in oil recovery operations or in other systems involving porous media. For single-phase fluids, oscillatory forcing might be employed to increase the mean flow rate, or it could be used as the sole means of inducing a mean flow. For two-fluid systems, the oscillatory forcing could be utilized as an *oscillatory filter* inducing a separation based on differences in fluid viscosity. In this mode, a spike waveform with large  $F_{rms}$  would be used to force the less viscous fluid to flow against the direction of the mean pressure gradient. At the same time, the more viscous fluid would experience a lower level of dimensionless forcing  $F_{rms}$  and hence flow in the direction of the mean forcing. This mechanism could be exploited in oil-water systems encountered in secondary oil recovery to reduce or even reverse the flow rate of water in the vicinity of the production wells. The end result would be a significant increase in the concentration of oil in the product streams.

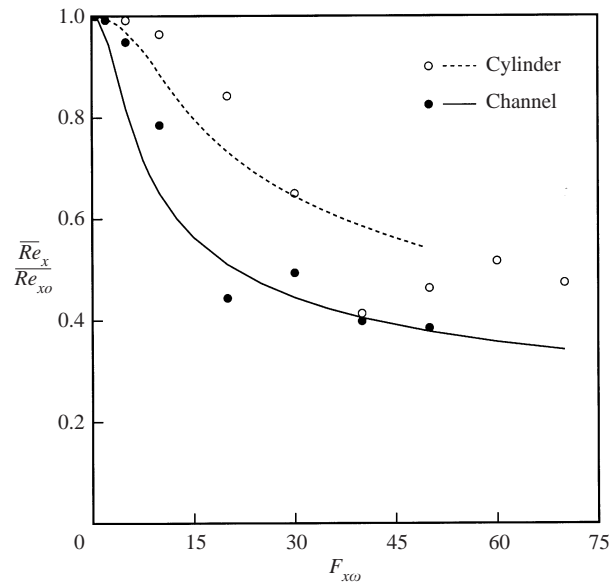


FIGURE 16. Mean flow rate as a function of oscillatory forcing level for fixed steady forcing  $F_{x0} = 0.25$ . The lines on the plot indicate quasi-steady analysis and the symbols are results of unsteady simulations at  $\Omega = 0.25$ .

### 3.3. Cross-flow forcing

Our previous analysis of oscillatory forcing has been restricted to the case of oscillations along the same axis as the mean forcing. This restriction is reasonable for the constricted channel model, because the impermeable top and bottom boundaries eliminate any influence of transverse forcing on the fluid flow field. Transverse body forces act solely to induce a hydrostatic pressure variation in the fluid. To investigate the effects of oscillatory forcing in a more general system, we consider periodic cylinder arrays with cross-flow forcing, where the axis of the oscillatory forcing is normal to the direction of mean forcing. In this system, we shall focus our attention on temporal waveforms restricted to simple sinusoidal profiles. Before presenting the results for cross-flow forcing, we briefly examine the case of parallel forcing to verify that the flow behaviour observed for constricted channels carries over to the cylinder array model. Figure 16 shows that the constricted channels and cylinder arrays show quite similar behaviour for the influence of the sinusoidal forcing. In each case, strong oscillatory forcing leads to a marked reduction in the mean flow rate, with a somewhat stronger influence in the case of the constricted channels.

Having verified that both models yield similar predictions for oscillatory forcing parallel to the direction of mean forcing, we now examine the case of oscillatory forcing normal to the direction of mean forcing. In figure 17, the solid lines show the quasi-steady predictions for the flow rate in the  $x$ -direction as a function of the strength of the oscillatory forcing in the  $y$ -direction,  $F_{y\omega}$ , for different levels of steady forcing  $F_{x0}$ . For the curves with low levels of steady forcing, the oscillatory forcing has a profound effect on the mean flow rate, but this effect lessens as the level of steady forcing is increased. The basis for this dramatic increase in flow rate can be seen by examining the bifurcation diagram for steady cross-forcing shown in figure 14 of Part 1. In that figure, we showed that the strong cross-flow jets which develop at moderate Reynolds number have a significant impact on the flow rate in the  $x$ -direction. To see if the

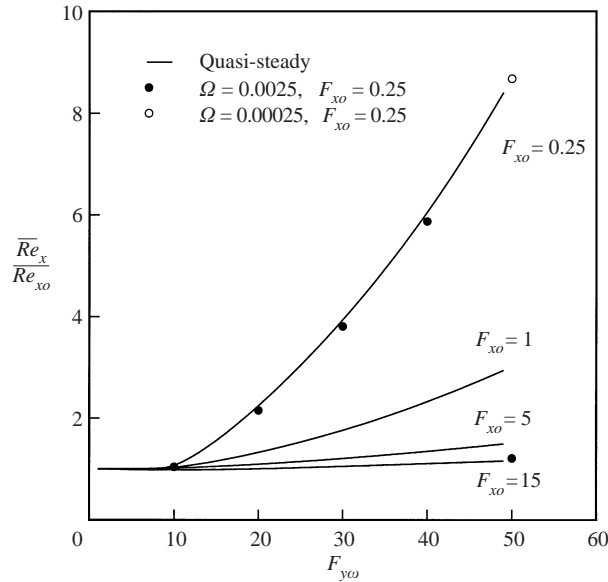


FIGURE 17. Mean flow rate as a function of cross-flow oscillatory forcing level  $F_{y\omega}$  for several levels of mean axial forcing  $F_{x0}$ .

quasi-steady predictions are borne out in the unsteady flows, we turn to the results for unsteady simulations shown as the symbols in figure 17. We show results for two different frequencies, with solid circles corresponding to  $\Omega = 0.0025$  and the open circle representing  $\Omega = 0.00025$ . The higher frequency results (solid circles) follow the quasi-steady prediction quite closely until the oscillatory forcing reaches a level of  $F_{y\omega} = 40$ , after which the flow rate drops sharply to a level close to its steady value in the absence of oscillatory forcing. For the lower frequency (open circle), the predictions of the quasi-steady theory remain valid to a higher level of oscillatory forcing. We conclude that the maximum frequency for which quasi-steady predictions are valid is a function of the oscillatory forcing level.

We may investigate the frequency dependence further by calculating the mean flow rate as a function of frequency for a fixed level of oscillatory forcing. The results are shown in figure 18. For the lowest frequencies, the average flow rate in the  $x$ -direction is increased by more than a factor of 2; however, for slightly higher frequencies ( $\Omega > 0.01$ ), the average flow rate decreases drastically and approaches the value corresponding to steady forcing. At higher frequencies ( $0.04 \leq \Omega \leq 0.05$ ), the cross-flow forcing reduces the flow rate below its steady forcing level, while for all frequencies above  $\Omega = 0.10$ , the cross-flow forcing has negligible effect on the mean flow rate. The explanation for these trends may again be found by examining the steady-flow results shown in Part 1. Recall that pure cross-flow forcing may lead to a net flow in the  $x$ -direction, but the direction of that induced flow may be positive or negative with equal likelihood. With oscillatory cross-flow forcing, the sense of the asymmetric streamline patterns may alternate yielding either an enhancement or reduction in the mean flow rate. This explains the different qualitative trends observed at different frequencies. While the changes in flow behaviour at the different frequencies may be of physical interest, an important result for practical application is that there is negligible effect above a frequency of  $\Omega = 0.10$ . Delivery of strong oscillatory forcing to porous media at extremely low frequencies is difficult because

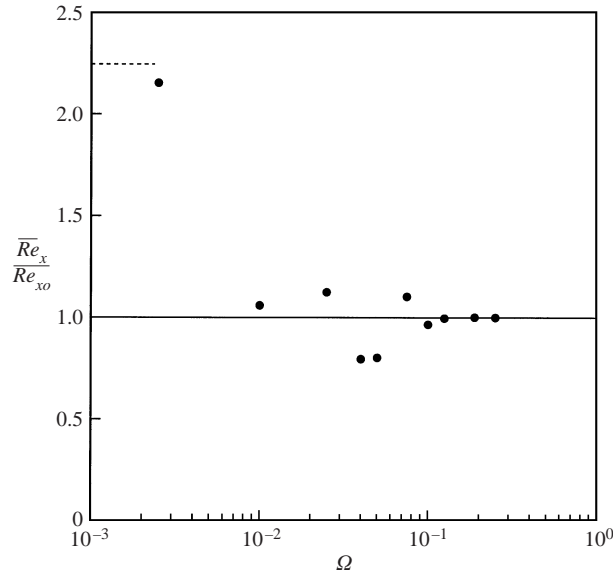


FIGURE 18. Mean flow rate as a function of frequency for fixed level of cross-flow forcing  $F_{y\omega} = 20$  and axial forcing level  $F_{x0} = 0.25$ .

it requires the creation of oscillations with extremely large displacements. Given the uncertainty in the results and the difficulty in administering strong oscillatory forcing, we conclude that cross-flow forcing is unlikely to provide a practical means of enhanced transport in porous media.

#### 4. Discussion

In the sections above, we have shown that inertial effects associated with oscillatory forcing may have a profound effect on the mean flow rate in porous media. With strong forcing and the appropriate waveform, the oscillatory forcing may act to either increase or decrease the flow rate. Waveforms may be selected to drive the fluid in the direction opposite to the mean pressure gradient, and two fluids of different viscosity may even be driven in opposite directions. The principal question remaining is whether these phenomena could be exploited in practice, or if the range of forcing required to achieve significant inertial effects is beyond the limits of feasibility.

To answer these questions, we begin by considering conditions which might apply in a typical oil reservoir. We assume that the porous medium is characterized by a length scale  $h = 2 \times 10^{-5}$  m. The kinematic viscosity of water is roughly  $10^{-6}$  m<sup>2</sup> s<sup>-1</sup>. With these values, we place an upper limit on the frequency of  $f = 1000$  Hz which yields a dimensionless frequency  $\Omega = 0.4$ . For frequencies of this level and below, the acoustic forcing will have significant effect if the forcing is of sufficient magnitude. For a given transducer operating at a frequency  $f$  with displacement  $d$ , the acceleration is  $4\pi^2 df^2$  and the acoustic body force is  $G_\omega = 4\pi^2 \rho d f^2$ . The dimensionless force is given by

$$F_\omega = 4\pi^2 f^2 d h^3 / \nu^2. \quad (4.1)$$

For frequencies in the range of 1000 Hz, one may employ metal transducers using a magnetostrictive metal alloy such as Terfenol-D<sup>®</sup>. Standard transducers of this type

are available from commercial vendors with operating ranges of 0 to 2500 Hz and displacements as large as 70  $\mu\text{m}$ . Note that metallic transducers of this type do not need to be operated at their natural frequencies, which typically fall in the range 2–6 kHz. Choosing a typical displacement  $d = 30 \mu\text{m}$ , we find that such a transducer can produce an acoustic forcing level of approximately  $F_\omega = 9$ . This level is well within the range of significant acoustic enhancement for both the sinusoidal and spike waves. (Note that  $F_{rms} = 0.203F_\omega$  for the spike waves considered here.)

While the displacement amplitude at the transducer is of sufficient magnitude, there is of course significant decay in amplitude as the acoustic wave propagates through the porous medium. The length scale for the decay rate will be a function of the size of the driving unit and the material properties of the solid matrix. For a strong localized effect utilizing the *oscillatory filter* principle, one might employ metallic transducers located within a well. Alternatively for longer range effect, some researchers have proposed using powerful surface generators. Frequencies of 1000 Hz and lower are sufficiently small that large-scale mechanical oscillating equipment may be employed with displacements and driving surfaces significantly larger than those achievable with metallic transducers.

While our focus has been on the application of acoustic stimulation in oil reservoirs, we note that flow in porous media is also encountered in numerous industrial operations in the petrochemical industry. Examples include filtration, flow in packed beds and mould filling with fibrous composites. In these operations, the porous media are far more accessible, and the introduction of significant forcing levels by mechanical oscillation or metallic transducers is easily achievable. As a brief example, we consider the parameter values from above for gap size  $h = 2 \times 10^{-5} \text{ m}$  and kinematic viscosity  $\nu = 10^{-6} \text{ m}^2 \text{ s}^{-1}$ . We suppose that mechanical oscillation is employed with a frequency of 100 Hz and a displacement of 10 cm. Significantly higher values might be achieved by specialized equipment; however these values are characteristic of mechanical equipment, e.g. an automobile engine. Substituting these parameters into equation (4.1) yields a dimensionless force  $F_\omega = 316$  which is far greater than any force considered here. If one is interested in media with larger pore sizes, equivalent oscillatory forcing levels can be achieved with significantly lower frequencies or smaller displacements.

It is not our purpose here to evaluate the merits of competing technologies for the design of industrial equipment. Our goal is to show that it is at least plausible to construct devices which can generate significant Reynolds numbers and inertial effects for flow in real porous media. With the range of forcing levels achieved by these devices, oscillatory forcing may lead to significant modification of the flow rate of single-phase fluids.

## 5. Conclusions

In this paper, we have demonstrated a number of mechanisms by which oscillatory forcing might be employed to modify the transport rate of single-phase fluids in porous media. These mechanisms may be exploited in multiphase systems when the two fluid phases occupy separate regions of the porous medium with individual patches of fluid covering areas significantly larger than the typical pore size. The main conclusions of this paper are as follows:

(i) Oscillatory forcing of porous media modifies the fluid velocity field through the action of an unsteady body force. All changes to the mean flow rate in single-phase

Newtonian fluids depend upon nonlinear interactions arising from the inertial terms in the Navier–Stokes equations.

(ii) Oscillatory forcing with sinusoidal waveforms decreases the average flow rate when the forcing level is significantly larger than the mean pressure gradient. The magnitude of the flow reduction increases as the dimensionless forcing level  $F_{rms}$  increases. The dimensionless forcing level is a function of the fluid viscosity, density and the pore size.

(iii) The temporal waveform of the oscillatory forcing function has a dramatic impact on the effectiveness of the oscillatory forcing. A spike waveform is found to be significantly more efficient than a sinusoidal profile. The spike waveform may be employed to drive a mean flow in the absence of a mean pressure gradient. In combination with a mean pressure gradient, the spike wave can increase the mean flow rate several fold. When the oscillatory forcing acts to oppose the mean pressure gradient, the spike wave can reverse the flow direction and drive the fluid against the mean pressure gradient.

(iv) The effects of oscillatory forcing on the mean flow rate are independent of frequency for small values of the dimensionless frequency  $\Omega$ . Oscillatory forcing has negligible effect on the mean flow rate for dimensionless frequencies  $\Omega > 1$  for sinusoidal forcing and for  $\Omega > 0.5$  for spike waveforms.

(v) When fluids of different viscosities are subjected to the same level of oscillatory forcing, the fluid with the lower viscosity experiences a significantly higher level of dimensionless forcing ( $\sim 1/\nu^2$ ). Thus oscillatory forcing may be employed to modify the flow rate of one fluid (water) while having negligible effect on the motion of a more viscous fluid (oil).

(vi) Owing to the sensitivity to viscosity ratio, oscillatory forcing may be employed to act as an *acoustic filter* whereby two fluids in a porous medium may be driven in opposite directions based on differences in the fluid viscosity.

(vii) Cross-flow oscillatory forcing may be employed with the axis of the oscillatory body force normal to the desired direction of mean flow; however, limitations on the dimensionless frequency place severe practical constraints on this mode of operation.

Finally, we have identified a number of fluid dynamics mechanisms which might provide an explanation for the enhanced transport rates observed in field test and laboratory experiments on acoustic stimulation of secondary oil recovery. We cannot determine if these are the primary mechanisms in actual field tests; however, we can confirm that the hydrodynamics of Newtonian fluids provides one explanation independent of other physio–chemical phenomena.

This work was supported by a grant from the National Science Foundation. D. R. Graham acknowledges the support of a Computational Science and Engineering Fellowship from the University of Illinois. Computational resources were provided by IBM through the Shared University Resource Program at the University of Illinois, and by the National Center for Supercomputing Applications.

#### REFERENCES

- BIOT, M. A. 1956*a* Theory of propagation of elastic waves in a fluid-saturated porous solid. I. Low-frequency range. *J. Acoust. Soc. Am.* **28**, 168–178.
- BIOT, M. A. 1956*b* Theory of propagation of elastic waves in a fluid-saturated porous solid. II. Higher frequency range. *J. Acoust. Soc. Am.* **28**, 179–191.
- BURRIDGE, R. & KELLER, J. B. 1981 Poroelasticity equations derived from microstructure. *J. Acoust. Soc. Am.* **70**, 1140–1146.

- CHAMPMAN, A. M. & HIGDON, J. J. L. 1992 Oscillatory Stokes flow in periodic porous media. *Phys. Fluids A* **4**, 2099–2116.
- CHAPMAN, A. M. & HIGDON, J. J. L. 1994 Effective elastic properties for a periodic bicontinuous porous medium. *J. Mech. Phys. Solids* **42**, 283–305.
- GRAHAM, D. R. 1997 Steady and oscillatory flow through model porous media. MS thesis, University of Illinois.
- GRAHAM, D. R. & HIGDON, J. J. L. 2002 Oscillatory forcing of flow through porous media. Part 1. Steady flow. *J. Fluid Mech.* **465**, 213–235.
- GRESHO, P. M., LEE, R. L. & SANI, R. L. 1980 On the time-dependent solution of the incompressible Navier–Stokes equations in two and three dimensions. In *Recent Advances in Numerical Methods in Fluids* (ed. C. Taylor & K. Morgan), pp. 27–79. Pineridge Press.
- NISHIMURA, T. 1995 Oscillatory flow and mass transfer within asymmetric and symmetric channels with sinusoidal wavy walls. *Heat Mass Transfer* **30**, 269–278.
- RALPH, M. E. 1986 Oscillatory flows in wavy-walled tubes. *J. Fluid Mech.* **168**, 515–540.
- ROBERTS, E. P. L. & MACKLEY, M. R. 1996 The development of asymmetry and period doubling for oscillatory flow in baffled channels. *J. Fluid Mech.* **328**, 19–48.
- ROSENHEAD, L. 1963 *Laminar Boundary Layers*. Oxford University Press.
- SOBEY, I. J. 1980 On flow through furrowed channels. Part 1. Calculated flow patterns. *J. Fluid Mech.* **96**, 1–26.
- STEPHANOFF, K. D., SOBEY, I. J. & BELLHOUSE, B. J. 1980 On flow through furrowed channels. Part 2. Observed flow patterns. *J. Fluid Mech.* **96**, 27–32.